Title

Expression of two major isoforms of MYO7A in the retina: Considerations for gene therapy of Usher syndrome type 1B.

Authors

Gilmore, W
Hultgren, Nan
Chadha, Abhishek
et al.

Publication Date

2023-11-01

DOI

10.1016/j.visres.2023.108311

Peer reviewed

HHS Public Access

Author manuscript

Vision Res. Author manuscript; available in PMC 2024 May 01.

Published in final edited form as:

Vision Res. 2023 November ; 212: 108311. doi:10.1016/j.visres.2023.108311.

Expression of two major isoforms of *MYO7A* in the retina: considerations for gene therapy of Usher syndrome type 1B

W. Blake Gilmore[1], **Nan W. Hultgren**[1], **Abhishek Chadha**[1], **Sonia B. Barocio**[1], **Joyce Zhang**[1], **Oksana Kutsyr**[2], **Miguel Flores-Bellver**[2], **M. Valeria Canto-Soler**[2], **David S. Williams**[1]

[1]Department of Ophthalmology and Stein Eye Institute, Department of Neurobiology, David Geffen School of Medicine at UCLA, Los Angeles, CA, USA,

[2]CellSight Ocular Stem Cell and Regeneration Research Program, Department of Ophthalmology, Sue Anschutz-Rodgers Eye Center, University of Colorado, School of Medicine; Aurora, CO, USA.

Abstract

Usher syndrome type 1B (USH1B) is a deaf-blindness disorder, caused by mutations in the *MYO7A* gene, which encodes the heavy chain of an unconventional actin-based motor protein. Here, we examined the two retinal isoforms of *MYO7A*, IF1 and IF2. We compared 3D models of the two isoforms and noted that the 38-amino acid region that is present in IF1 but absent from IF2 affects the C lobe of the FERM1 domain and the opening of a cleft in this potentially important protein binding domain. Expression of each of the two isoforms of human *MYO7A* and pig and mouse *Myo7a* was detected in the RPE and neural retina. Quantification by qPCR showed that the expression of IF2 was typically ~7-fold greater than that of IF1. We discuss the implications of these findings for any USH1B gene therapy strategy. Given the current incomplete knowledge of the functions of each isoform, both isoforms should be considered for targeting both the RPE and the neural retina in gene augmentation therapies.

Keywords

MYO7A; Usher syndrome; retina; isoforms; gene therapy

1. Introduction

Retinal degenerations (RDs) due to monogenic mutations occur at a frequency of approximately, 1 in 2000, worldwide (Berger et al., 2010). Most of these degenerations (70% according to RetNet) are recessively inherited, caused by loss of gene function, so that the disease can potentially be treated by the introduction of a normal (WT) copy of the mutant gene. Such gene augmentation therapies have now been attempted for numerous genes, with one FDA-approved product so far; in 2017, approval was given for treating a form of Leber congenital amaurosis (LCA2), which is caused by biallelic mutations in

*Corresponding author: David S. Williams, Department of Ophthalmology and Stein Eye Institute, Department of Neurobiology, David Geffen School of Medicine at UCLA, Los Angeles, CA, USA, dswilliams@ucla.edu.

No financial interests or conflicts of interest

RPE65, by delivering WT *RPE65* to the RPE with adeno-associated virus (AAV) (Russell et al., 2017). Similar approaches for several other inherited RDs are in clinical trials (Rakoczy et al., 2019, Cehajic-Kapetanovic et al., 2020, Fischer et al., 2020, Yu-Wai-Man et al., 2020).

A limitation of gene therapy, whether by augmentation or in situ editing of the mutation, is that the retinal cells need to be treated before there is too much degeneration, as it is dependent on the presence of healthy cells to start expressing the introduced WT copy of the gene. In LCA2 cases, administration of treatment in older patients has been found to be less efficacious in the long term (Cideciyan et al., 2013). This limitation means that patients should be identified before manifestation of retinal disease. LCA2 patients are born blind due to disruption of the visual cycle, so that young patients can be potentially identified before the onset of RD. However, for many other inherited RDs, pending blindness is only noticed once there is loss of peripheral vision, which may not occur until a significant portion of photoreceptor cells have degenerated or at least have been damaged.

Usher syndrome (USH) is a deaf-blindness disorder, caused by recessive mutations in any one of numerous autosomal genes, nine of which have been identified and confirmed (Williams, 2008, Castiglione & Moller, 2022). The deafness precedes RD and is most obvious in USH1 patients, who are born profoundly deaf. Most of these patients are now treated with cochlear implants to address their deafness. The early identification of these patients, before the onset of RD, means that USH patients represent a highly suitable population for retinal gene therapy.

Commonly, gene augmentation approaches involve the delivery of a single cDNA of the WT gene. Despite the successes of this approach, it is potentially limited in cases where the mutant gene normally expresses more than one isoform. Previously, we noted that most of the USH genes might express more than one isoform (Williams et al., 2017).

Here, we focused on retinal isoform expression of the most common USH1 gene, *MYO7A*, which underlies USH1B (Weil et al., 1995). *MYO7A* encodes the heavy chain of an actin-based motor protein (Udovichenko et al., 2002). Our results show that the neural retina and RPE from human, pig, and mouse all express two isoforms of *MYO7A*. We discuss the relevance of our findings to USH1B gene therapy approaches.

2. Materials and Methods

2.1. Human and animal tissues

C57BL6 mice carrying WT *Myo7a* on both alleles were maintained as described (Gibbs, et al 2003). Young mice, aged postnatal day 9–15, were used due to the relative ease of separation of RPE from neural retina. Mouse NR samples were comprised of pooled tissues from each eye to ensure sufficient RNA yields. To obtain sufficient material for analysis, mouse RPE was cultured and expanded for 3–5 days. These primary mouse RPE samples were combined when harvesting RNA. Pig eyes were obtained through UCLA Division of Laboratory Animal Medicine (DLAM). Eyes were excised from the eye socket and dissected to expose the tissues of the retina. The neural retina was separated from the eyecup and set aside for further processing. The RPE layer was carefully isolated from the eyecup by

mechanical separation. De-identified samples of post-mortem posterior eye segments (from a 42-year old male and a 90-year old female, neither with any known retinal disease) were provided by the laboratory of Dr Gabriel Travis, at the Stein Eye Institute, according to regulations for anonymous pathological specimens. All tissue samples were immediately processed following isolation, or otherwise flash frozen and stored at −80°C.

2.2. Cell culture

ARPE-19 cells were thawed and cultured in DMEM/F12 with GlutaMAX, 10% FBS, 100 U/mL Penicillin and 100 U/mL Streptomycin, until confluency was reached. Cells were then passaged and seeded into a new culture plate (1.66×10^5 cells/cm^2) with differentiation medium (MEM-Nic with GlutaMAX, 1% FBS, 100 U/mL Penicillin, 100 U/mL Streptomycin, 1% N1 supplement, 0.1 mM NEAA, taurine (0.25 mg/ml), hydrocortisone (20 ng/ml), triiodo-thyronine (0.013 ng/ml), and 10 mM nicotinamide) (Hazim et al., 2019, Hazim et al., 2022). The cells were maintained for at least 14 days at 37°C, 5% CO_2 with media changes every 2–3 days until a polarized morphology was established.

The H9 embryonic stem cell line used in these studies was generated by WiCell (Madison, Wisconsin), and provided for our studies through the UCLA Broad Stem Cell Research Center Stem Cell Bank. The xcHUF1 iPS cell line was also obtained through the UCLA Stem Cell Bank facility, where the line was generated by lentiviral cassette integration of the reprogramming factors Oct4, Sox2, Klf4, and cMyc. This line originated from an individual with no known retinal disease, and was used only for isolated iPSC-RPE cultures.

All stem cells were plated and maintained on Matrigel® Basement Matrix-coated tissue culture plates and cultured in mTeSR™1 Basal Medium. Differentiation from pluripotent state into RPE was performed using a described 14-day differentiation protocol (Buchholz et al., 2013) with modifications (Hazim et al., 2017). Briefly, plated ESC or iPSC colonies were cultured for days 0 and 1 in basal medium supplemented with Noggin (50 ng/mL), Dkk1 (10 mg/mL), and IGF1 (10 mg/mL). On day 2, the culture media is replaced with basal medium supplemented with Noggin (10 ng/mL), Dkk1 (10mg/mL), and IGF1 (10 mg/mL), and bFGF (5 ng/mL). On day 4, the medium is again replaced, this time with basal medium supplemented with Dkk1 (10 ng/mL) and IGF1 (10 ng/mL). For days 4 through 14, differentiating cultures were maintained in fresh basal medium supplemented with Activin A (100 ng/mL) and SU5402 (10 μM). Finally, after 14 days, culture media is switched to MEM-Nic with 5% FBS, and replaced every 2–3 days until pigmented, cuboidal RPE cells begin to appear within the culture. These patches of RPE were mechanically isolated, and expanded into homogenous hiPS-RPE or hES-RPE cultures.

Retinal organoids were generated from an hiPSC line derived from $CD34^+$ cord blood (A18945, Thermo Fisher Scientific) (Burridge et al., 2011). The karyotype of this cell line was verified to be normal. Undifferentiated hiPSCs and derived retinal organoids were routinely tested to confirm the absence of contamination by mycoplasma (PCR Universal Mycoplasma Kit, ATCC), bacteria and fungi. Cell culture, retinal differentiation, and organoid formation were conducted as described previously (Zhong et al., 2014, Aparicio-Domingo et al., 2023). Retinal organoids at 270 days of differentiation were used for these

studies. Induced primary RPE were obtained from retinal organoids (ro-RPE), as described (Flores-Bellver et al., 2021). Briefly, RPE tissue was isolated from retinal organoids at 60 days of differentiation, and then enzymatically dissociated into single cells, and seeded on to Transwell culture membrane inserts (No. 3460, Corning), coated with Matrigel matrix (No. 354230, Corning). RPE cells were maintained at 37°C and 5% CO_2 in MEM-Nic as described above but with 5% FBS, as described previously (Maminishkis et al., 2006), until they were fully differentiated.

2.3. Isoform-specific full length cDNA construct cloning and sequencing analysis

Full length *MYO7A*/*Myo7a* was PCR amplified from RPE samples using the following primers:

hMYO7A Forward: 5'-ATGGTGATTCTTCAGCAGGGG-3'

hMYO7A Reverse: 5'-TCACTTGCCGCTCCTGGA-3'

mMyo7a Forward: 5'-ATGGTTATTCTGCAGAAGGGGG-3'

mMyo7a Reverse: 5'-TCACCTTCCACTCCTGGAGT-3'

pMyo7a Forward: 5'-ATGGTGATTCTTCAGCAGGGG-3'

pMyo7a Reverse: 5'-TCACTTGCCACTCCTGGAG-3'

The resulting amplicons were submitted for Sanger sequencing (Laragen, Culver City, CA), using the sequencing primer IFID Forward (5'-AAGGGGATTTATGCCCAGAG-3'). The resulting chromatograms were viewed using SnapGene software (San Diego, CA).

Human and mouse *Myo7a* PCR products were cloned into TOPO backbone plasmid using the TOPO TA Cloning kit (ThermoFisher), transformed into competent bacteria, and plated onto LB agar plates supplemented with Kanamycin (50μg/mL). Clonal transformants were grown up in LB + Kanamycin cultures. Plasmid DNA was purified by Purelink Quick Plasmid Miniprep Kit (Invitrogen). Purified plasmid DNA was submitted for Sanger sequencing (Laragen, Culver City, CA)

2.4. Sample preparation for quantitative PCR

The expression of *MYO7A* or *Myo7a* in collected samples was verified using quantitative reverse transcription-PCR (qRT-PCR). Total RNA was extracted from samples using the RNeasy Mini Kit (Qiagen), as described by the manufacturer's protocol. Fully polarized ARPE-19 cells were washed twice with PBS prior to harvest, and then mechanically scraped from the culture well for RNA extraction. Samples of RPE from retinal organoids (ro-RPE) were incubated in RNA Protect (Qiagen, Hilden, Germany) to attenuate endogenous RNase activity and mRNA synthesis, and then scraped off the plate into a 1.5-ml tube. Cells were centrifuged at 2500 × *g* for 10 min and the pellet was resuspended in buffer RLT plus (RNeasy Plus Micro/Mini Kits; Qiagen) with 2-mercaptoethanol (1:100; Sigma–Aldrich Corp.). In the case of retinal organoids, neural retina devoid of RPE was used. Retinal organoid samples were washed twice with PBS and then incubated with 150 μL of TRIzol

reagent (Thermo Fisher Scientific, USA) for 5 min. at room temperature (RT). The mixture was vortexed well to ensure complete lysis of the tissue. This was followed by the addition of 30 μL of chloroform (Sigma Aldrich, USA), vigorously shaken, and incubated for 3 min at RT. Samples were then centrifuged for 5 min at 12000 × g at 4°C to separate the phases. The aqueous phase was collected carefully, so not to disturb the interphase, and dispensed into another microtube for further RNA processing. Primary mouse and pig tissues were collected and homogenized, then passaged through a syringe to facilitate dissociation. Purified RNA was eluted from the column with a maximum of 40 μL Ultrapure RNase-free water or elution buffer, and then analyzed by nanodrop to determine concentration. RNA concentration was generally standardized to 100 ng/μL or 250 ng/μL. Purified total RNA (1–2 μg) was used immediately for first strand cDNA synthesis or otherwise stored at −80°C. Purified RNA was reverse transcribed into cDNA using Superscript IV First Strand Synthesis Kit (Thermo Fisher) according to the manufacturer's protocol. To ensure that cDNA was generated from only messenger RNA, we opted for the oligo d(T) primer during synthesis. Samples were stored at −20°C until qPCR analysis.

2.5. Quantitative PCR primers

The following primer sets were used for amplification of *MYO7A, Myo7a*, or housekeeping genes:

hMYO7A qPCR IF1&2 Forward: 5'-CCCAAGAACGACGTCATC-3'

hMYO7A qPCR IF2 Reverse: 5'-GTTTTCGCTCCCCTGCT-3'

hMYO7A qPCR IF1 Reverse: 5'-GCAGCACAGCCAAGATCA-3'

hHPRT Reverse: 5'-CCCTGTTGACTGGTCATTACA-3'

hHPRT Forward: 5'-GGAGGCGATCACATTGTA-3'

mMyo7a IF1&2 Set 1 Reverse: 5'-CCAGCAGGGTTAGGATTGT-3'

mMyo7a IF1 Set 1 Forward: 5'-GGGCTGTGCTACTTGTCAA-3'

mMyo7a IF2 Set 1 Forward: 5'-GTGTCCAGCAGTAGGGGAACA-3'

mMyo7a IF1 Set 2 Forward: 5'-CCCAAGAGCGACGTCATC-3'

mMyo7a IF1 Set 2 Reverse: 5'-GTAGCACAGCCCAAGTCAG-3'

mHprt Forward: 5'-GGTGGAGATGATCTCTCAACTT-3'

mHprt Reverse: 5'-CTGGCCTGTATCCAACACTT-3'

pMyo7a IF1&2 Forward: 5'-AGCCTCCCCAAGAATGATGT-3'

pMyo7a IF1 Reverse: 5'-CAGGACCAACACGAAGAACA-3'

pMyo7a IF2 Reverse: 5'-GGTTCGCTCCCCTGCT-3'

pHprt Forward: 5’-GGACTTGAATCATGTTTGTG-3’

pHprt Reverse: 5’-CAGATGTTTCCAAACTCAAC-3’

2.6 Quantitative PCR standardization

MYO7A and *Myo7a* primers were designed to span exon-exon junctions specific to each isoform to ensure that amplification was isoform specific, as well as to avoid amplification of genomic DNA. Standard curves were performed with each *MYO7A* or *Myo7a* primer set to ensure resulting data were not biased by differences in primer efficiency.

Two types of mouse samples were used as template: mouse RPE cDNA, or, alternatively, full length *Myo7a* cloned into a pTOPO backbone plasmid. Full length *Myo7a* was PCR amplified from mouse RPE cDNA and the PCR products were cloned into a plasmid backbone using the Zero Blunt™ TOPO™ PCR Cloning Kit (Invitrogen). Clones were screened by Sanger sequencing (Laragen, Culver City, CA) to obtain isoform specific template vectors. The resulting templates (pTOPO-mus*Myo7a*-IF1, pTOPO-mus*Myo7a*-IF2) were prepared using PureLink™ Quick Plasmid Miniprep Kit (Invitrogen). Human samples from previously prepared plasmid DNA, containing either *MYO7A* IF1 or IF2, were also tested (pUH-CBA-mCherry-MYO7A-IF1, pUH-CBA-mCherry-MYO7A-IF2).

The qPCR reactions were prepared in triplicate with each serial dilution, as follows: 1 μL DNA template, 1 μL 10uM Forward and Reverse primer, 10 μL SYBR Green Master Mix, and 8 μL Ultrapure RNase-free water for a total of 20uL per reaction. Samples were loaded into individual wells of a 96-well qPCR plate and analyzed using the Quant Studio 3 Pro Real-Time PCR System (Applied Biosystems). Ct values were averaged for each sampling group and plotted against the log of the DNA copy number (Supplemental Fig. 2). Amplification efficiencies were calculated (Eff = $10^{(-1/\text{slope})} - 1$) and recorded beneath each plot.

2.7 Quantitative PCR primer isoform specificity

Quantitative PCR analysis using templates made of pure isoform-specific cDNA plasmids at different concentrations, as well as mixtures of both IF1 and IF2 cDNA plasmids at various ratios were conducted for each primer set. The qPCR conditions used in the actual experimental conditions, as described above, were used. The average Ct value for each condition is the mean of three technical replicates.

2.8 Quantitative PCR analysis

Quantitative PCR amplification was performed using SYBR Green Master Mix (Applied Biosystem or BioRad). Fluorescent detection of PCR amplification was analyzed using Quant Studio 3 Pro Real-Time PCR System (Applied Biosystems) or LightCycler 480 Real-Time PCR Thermal Cycler (Roche), or Q qPCR instrument (Quantabio) with the following program: 50°C for 2 min, 95°C for 10 min, 40 cycles of 95°C for 15 sec followed by 60°C for 1 min. Melt curve analysis was performed to determine specificity of each PCR reaction, as follows: 95°C for 15 sec, 60°C for 1 min, and then 10 sec incremental incline of 1°C, up to 95°C. The housekeeping gene, *HPRT*, was used as an internal control.

The relative expression of *MYO7A* IF1 and IF2 was determined by calculating ΔΔCt, normalized to *HPRT* expression. The Ct value was determined for each PCR reaction by automated threshold analysis by the PCR instrument, Quant Studio 3 Pro Real-Time PCR System (Applied Biosystems), LightCycler 480 Real-Time PCR Thermal Cycler (Roche), or Q qPCR instrument (Quantabio). Samples containing impurities, as determined by melting curve analysis, were discarded from analysis. The value of each technical replicate within a sample group was calculated and normalized to the housekeeping gene as such: ΔCt (*MYO7A*) = Ct(*MYO7A*)- Ct(*HPRT*). The ΔΔCt was calculated from the difference in each normalized *MYO7A* ΔCt, as ΔΔCt = ΔCt(*MYO7A* IF1) - ΔCt(*MYO7A* IF2). Finally, the relative expression of each isoform was represented by $2^{-\Delta\Delta Ct}$.

2.9 Quantitative PCR sample sizes

As shown in Table 1, eleven mouse neural retina samples, each consisting of two pooled retinas, and four mouse RPE samples, each consisting of tissues pooled from four mice, were collected for analysis. An NR and RPE sample were each collected from two pig eyes. Seven wells of ARPE-19 were each independently polarized and harvested for analysis. Four cultures of differentiated RPE from xcHUF1 hiPSCs, and two cultures from hESCs were sampled. Data collected from stem cell-derived RPE samples were combined into a single group (iPS/ES-RPE) for analysis. Five groups of retinal organoids were used for analysis, each group containing a pool of six organoids. Four biological replicates of ro-RPE were used for analysis. Two de-identified post-mortem human subject eyes were collected, one each from two adult subjects. Both NR and RPE were sampled from the 42-year old subject, while just the RPE was sampled from the 90-year old subject. Between three and six technical replicates were used for each data point, depending on the RNA yield of each sample.

2.10. 3D modeling

3D models were generated by the Pymol software (https://pymol.org/2/). Myosin 7a FERM1 and FERM2 domains amino acid sequences were analyzed using the Phyre2 webserver (http://www.sbg.bio.ic.ac.uk/phyre2), or otherwise obtained from the Protein Data Bank (https://www.rcsb.org/). The resulting model (.pcb format) was imported into Pymol for 3D visualization analysis.

3. Results

In a screen of a human retinal cDNA library, multiple independent clones were found to represent one of two isoforms of *MYO7A*, which differed by the presence or absence of a 114-bp region (Weil et al., 1996). We detected these two isoforms in full length *Myo7a* or *MYO7A* PCR amplicons from mouse, pig and human RPE samples, using Sanger sequencing (Suppl. Fig. 1A). After cloning these cDNA libraries to generate pure isoform-specific constructs, we sequenced individual clones to determine the frequency of clones containing each isoform. In mouse RPE, we detected 1 clone containing the larger isoform and 5 independent clones containing the 114-bp deletion. In human RPE, we detected 2 independent clones of the larger isoform and 12 of the smaller isoform (Suppl. Fig. 1B). We refer to the larger isoform as IF1, and the smaller as IF2.

Fig. 1A depicts the domains of MYO7A and illustrates that the two isoforms differ from each other by a 38 amino acid sequence that is present in IF1 but not IF2. The presence or absence of this sequence is due to alternative splicing of exon 35, and it affects the structure of the FERM1 domain in the MYO7A tail (Fig. 1).

FERM domains are common protein binding regions (Chishti et al., 1998), so that any changes in these regions are likely to affect specific protein function. Some binding partners to the FERM1 domain of MYO7A have been reported, including another Usher 1 protein, SANS (Adato et al., 2005). To investigate the structural implications of modifying this domain, 3D models of each isoform were generated. These models revealed differences in the amino acid sequences at the tip of one loop of the C-lobe of the FERM1 domain. The differences appear to affect the opening to the cleft created between different lobes, and are thus likely to result in different protein interactions between IF1 and IF2 (Fig. 1D).

In the retina, MYO7A has been detected in the RPE and the photoreceptor cells of rodents and humans by immunocytochemistry (Hasson et al., 1995, Liu et al., 1997). Mutant phenotypes in mice, lacking functional MYO7A, confirm this localization by showing functions for MYO7A in both these cell types (e.g. Liu et al., 1998, Liu et al., 1999). Single cell RNA sequencing of human retinal organoids has also detected the expression of *MYO7A* in Müller cells and on-bipolar cells (Leong et al., 2022), although no MYO7A protein has been demonstrated in these cells.

To determine the relative abundance of each isoform in RPE and neural retina (NR, including the photoreceptor cells), we compared the relative expression of IF1 and IF2 in a variety of RPE and NR samples from mouse, pig, and human. The mouse and pig samples consisted of freshly dissected post-mortem retinas. The human RPE samples included cultures of polarized monolayers that were differentiated from 1) the ARPE-19 cell line, 2) human embryonic stem cells (hESCs), and 3) human induced pluripotent stem cells (hiPSCs). The human NR samples included retinal organoids that were generated from hiPSCs, and polarized RPE that was isolated and further differentiated from the retinal organoids (ro-RPE). In addition, we tested NR and RPE from human post-mortem eyes.

To ensure the comparison of IF1 and IF2 expression level would not be skewed by a difference in primer efficiency, we generated standard curves for human and mouse primer sets using species- and isoform-specific cDNA constructs. Due to the short sequence difference between the two isoforms (114 bp), primer design options were limited. However, the primers we selected had a comparable efficiency between IF1 and IF2 for each species (0.77 and 0.79 for mouse, and 0.83 and 0.85 for human, Suppl. Fig. 2). To further test the specificity of each primer set, we conducted qPCR analysis using a mixture of both isoform-specific cDNA plasmids; we found relatively negligible amplification of the non-targeted isoform template at the measured expression ratios (Supplementary Tables 1 and 2).

The ratio of IF1 to IF2 was relatively consistent for the different human and pig samples tested (Fig. 2). IF2 was the predominant isoform expressed in human RPE and NR samples, accounting for 82–90% of the relative *MYO7A* expression. A similar isoform ratio was found in pig tissues, with IF2 accounting for the majority of expression in both the RPE

(89%) and NR (90%). On average, IF1 accounted for about 1 in 7 of *MYO7A* transcripts across pig and human samples, a ratio that is consistent with the frequency of isoform-specific clones from the human samples (Suppl. Fig. 1B). In mouse RPE, IF1 was still the lower expressed isoform, but accounted for a larger relative proportion of *Myo7a* transcript (23%). In contrast, mouse NR showed higher expression of IF1 than IF2 expression (52 vs 48%).

4. Discussion

Like most of the other Usher syndrome genes (Williams et al., 2017), *MYO7A* is alternatively spliced, with two major isoforms expressed in the retina (Weil et al., 1996). Using quantitative PCR, we measured significant expression of both these two isoforms in the NR and RPE of human, pig and mouse. In human and pig NR and the RPE of all three species, the expression of IF2 was greater than that of the longer form, IF1. In mouse NR, IF1 expression was more comparable to that of IF2. Irrespective of the relative expression levels of the two isoforms, an important point from our study is that significant levels of both isoforms were detected in both the NR and the RPE of three different mammals. This finding suggests that both IF1 and IF2 of MYO7A likely function in the developed NR and RPE, so that gene augmentation therapy attempts with a single isoform might be of limited success.

4.1. Retinal MYO7A isoforms in relation to gene augmentation therapy

The first clinical trial to prevent USH1B blindness used gene augmentation therapy with *MYO7A* IF2. Based on our relative expression data, this more highly expressed isoform would seem to have been a more prudent choice – if only one isoform were to be used. The human IF2 construct was provided by our lab to Oxford Biomedica for incorporation into an EIAV lentiviral vector for subretinal delivery. This trial was abandoned before efficacy could be assessed properly. Nevertheless, earlier, HIV lentiviral delivery of the same IF2 construct had been shown to correct some of the known mutant phenotypes due to lack of MYO7A function in mouse retinas. Correction was determined by the localization and motility of RPE melanosomes, the degradation of photoreceptor outer segment phagosomes, and the concentration of opsin in the connecting cilia of the photoreceptor cells (Hashimoto et al., 2007). *Myo7a*-mutant mice manifest mislocalized melanosomes in the apical RPE, due to aberrant motility (Liu et al., 1998, Futter et al., 2004, Gibbs et al., 2004), slowed phagosome degradation, due to impaired movement of the nascent phagosomes from the apical RPE (Gibbs et al., 2003, Jiang et al., 2015), and an abnormal accumulation of opsin in the connecting cilia of photoreceptor cells (Liu et al., 1999). However, lack of MYO7A also results in several additional mutant phenotypes, which suggest other functions (Williams & Lopes, 2011).

Electrophysiological studies of *Myo7a*-mutant mice showed a slightly reduced a- and b-wave response (Libby & Steel, 2001). With mutant mice on a different genetic background, a more significant electroretinogram abnormality was observed, including a delay in the recovery of rod responsiveness after desensitization (Colella et al., 2013). In the RPE, MYO7A is also required for the light-dependent translocation of the retinoid isomerase,

RPE65, with mice that lack MYO7A having lower overall levels of RPE65, as well as mislocalization of the isomerase (Lopes et al., 2011). Correction of these phenotypes was not tested in the initial gene augmentation studies in mice (Hashimoto et al., 2007); nor were they tested in a later study using the same IF2 cDNA, but delivered by AAV (Lopes et al., 2013).

Interestingly, gene augmentation studies with *Myo7a*-mutant mice, using a cDNA of human *MYO7A* IF1, have demonstrated correction of some of the same phenotypes that were corrected by human *MYO7A* IF2. Melanosome localization in the apical RPE was corrected with human *MYO7A* cDNA that was reported to be IF1, packaged in either single or dual AAV vectors (Colella et al., 2013, Trapani et al., 2014, Ferla et al., 2023). This treatment also improved the electrophysiological recovery from light desensitization (Colella et al., 2013).

The correction of melanosome localization with either IF1 or IF2 is consistent with the reported interaction between MYO7A and melanosomes in the RPE. Melanosome motility by MYO7A is mediated by association of RAB27A on melanosomes with the exophilin, MYRIP, which in turn binds to a region of the tail of MYO7A (El-Amraoui et al., 2002, Fukuda & Kuroda, 2002, Klomp et al., 2007, Lopes et al., 2007). This tail region of MYO7A is identical between MYO7A IF1 and IF2. It includes the FERM2 domain, but it does not include the FERM1 domain, which is where the two isoforms differ (Fig. 1). The requirement of the MYO7A FERM2 tail region for melanosome motility and localization has been demonstrated in vivo, using *Myo7a*-mutant mice, known as *polka*. *Polka* mice carry a splice site mutation (c.5742+5G>A) that results in a MYO7A protein, truncated at the FERM2 domain. In the RPE of *polka* mice, the mutant MYO7A protein is present at WT levels, but it does not associate with melanosomes, resulting in their mislocalization (Schwander et al., 2009).

Functions that involve protein or organelle association with the FERM1 domain of MYO7A are more likely to be specific for IF1 or IF2. In this respect, the scaffolding protein, SANS, has been shown to bind the FERM1 domain of MYO7A (Adato et al., 2005). Mutations in *SANS* underlie USH1G (Weil et al., 2003), and SANS-MYO7A binding is thought to be part of a network of USH1 proteins (Adato et al., 2005, Reiners et al., 2005), and perhaps involved in ciliary transport (Sorusch et al., 2019).

In summary, MYO7A IF1 and IF2 are likely to have overlapping functions (e.g. melanosome motility and localization), in addition to distinct functions that involve the FERM1 domain. Although gene augmentation experiments with either IF1 and IF2 have corrected some mutant phenotypes in mice (Hashimoto et al., 2007, Lopes et al., 2013, Colella et al., 2014), correction of other mutant phenotypes has not been demonstrated. These other mutant phenotypes may result from loss of one specific isoform. To our knowledge, there are no known USH1B mutations that would affect just one *MYO7A* isoform. Nevertheless, two mutations in the IF1-specific region, a nonsense mutation, W1558X, and a frameshift mutation (2-bp deletion), C1554fs, have been reported by ClinVar (but with no ophthamological information); ClinVar is hosted by the National Center for Biotechnology Information (NCBI). With the possibility of requiring IF1 or IF2, specifically, to correct a

mutant phenotype (due to function related to the FERM1 domain of MYO7A), it seems prudent, to design a gene augmentation therapy that includes both isoforms. One approach would be to test a single construct with IF1 cDNA that includes intron 34 (0.9 kb), to potentially generate both IF1 and IF2 through alternative splicing (Fig. 3).

An alternative approach would be to employ gene editing, rather than gene augmentation. In general, gene editing assumes an advantage over gene augmentation when a gene expresses more than one isoform. A paper in this *Vision Research* special edition (Yan et al., 2023) argues for additional advantages. However, USH1B mutations are present in all parts of the *MYO7A* gene, with no particular mutation showing a high frequency (Jacobson et al., 2011), so that a significant advantage of a well-designed gene augmentation therapy for USH1B is that it should provide one treatment for all cases, whereas gene editing would not.

4.2. Both the RPE and photoreceptors as necessary targets for USH1B gene therapy

Previously, we reported that the photoreceptors might be the initial site of the USH1B disease, based on the first detection of cell pathology by in vivo imaging and the similarity of retinal pathology of USH1B with that of other Usher syndromes (Jacobson et al., 2008). However, more advanced imaging of RPE cells may have detected RPE pathology earlier. In any case, there are two fundamental reasons that suggest there is a need to address both the RPE and photoreceptors in USH1B gene therapy. First, MYO7A protein, as well as mutant phenotypes in its absence, have been detected in both mammalian RPE and photoreceptors (Hasson et al., 1995, Liu et al., 1997, Liu et al., 1998, Liu et al., 1999). Second, the site of manifestation of pathology is not necessarily the site of the defective molecular mechanism that leads to the evident pathology. There are several well-known examples among inherited RDs that involve cell nonautonomous impairment, particularly where a molecular defect in the RPE results in primary pathology in the photoreceptor cells; e.g. mutations in *MERTK* and *RPE65* (Mullen & LaVail, 1976, Gu et al., 1997). Moreover, the variety of mutant phenotypes due to a lack of MYO7A function in the retina suggests that these defects may collectively contribute to USH1B pathology. While these mutant phenotypes were largely discovered in mice, some have been corroborated in human RPE cells. For example, impaired degradation of phagosomes was shown in *MYO7A*-deficient human RPE cells (Gibbs et al., 2010). This particular cellular RPE defect is a good candidate for contributing to a general insult that leads to USH1B pathology, since it has been linked to RD through mutations in other genes (Rakoczy et al., 2002, Krock et al., 2007, Gordiyenko et al., 2010, Jiang et al., 2015, Esteve-Rudd et al., 2018).

Therefore, it seems clear that we should treat both the photoreceptors and the RPE in USH1B in any planned gene therapy – and, as noted above, the expression of MYO7A IF1 and IF2 in both the RPE and the NR indicates that treatment should address both isoforms. A question remains whether additional retina cell types should also be targeted. The detection of *MYO7A* gene expression in other retinal cells, by single cell RNA sequencing of human retinal organoids (Leong et al., 2022), suggests that these other cells, especially the Müller cells which provide a supportive role to the photoreceptors (Reichenbach et al., 1993), might also be a necessary target for complete retinal gene therapy.

4.3. Comparative localization of MYO7A in the photoreceptors

An early low magnification immunolabeling study of mouse photoreceptors failed to detect MYO7A (El-Amraoui et al., 1996), and a recent paper also concluded that MYO7A was absent from mouse photoreceptors (Calabro et al., 2019). However, immunoEM studies have not only been able to detect MYO7A in the connecting cilium, but also demonstrate the abnormal accumulation of opsin in this region in *Myo7a*-mutant mice, thus associating a mutant phenotype due to loss of MYO7A function with mouse photoreceptors. These EM results have now been verified independently by at least 4 different laboratories (Liu et al., 1997, Liu et al., 1999, Hasson, 2000, Wolfrum & Schmitt, 2000, Colella et al., 2013). Moreover, using female *Myo7a*-null mice, expressing a *Myo7a* transgene from their X-chromosome, it was demonstrated that the mutant phenotype of abnormal opsin accumulation in the connecting cilium is due to lack of MYO7A in the photoreceptor cells themselves and not from lack of MYO7A in the RPE cells; the retinas of these mice contained mosaics of MYO7A-null and MYO7A-positive photoreceptor and RPE cells (Jacobson et al., 2008).

ImmunoEM suggests that the localization of MYO7A to the photoreceptor connecting cilium is similar between human and rodents (Liu et al., 1997). However, MYO7A is also localized to the photoreceptor calycal processes, together with other USH1 proteins (Sahly et al., 2012), and the organization of the calycal processes differs significantly between mouse and human. A calycal process is an f-actin-filled extension from the inner segment that associates with the proximal region of the outer segment. Mouse and rat rod photoreceptors have been shown to possess at least a single calycal process (Kessel & Kardon, 1979, Arikawa et al., 1992, Volland et al., 2015). However, they do not possess the array of many calycal processes that surrounds the basal region of the outer segments of primates, pigs, frogs, and many other vertebrates (Brown et al., 1963, Hogan et al., 1971, Steinberg et al., 1980). Calycal processes require actin filaments for their organization. When f-actin is depolymerized, they collapse, and this collapse was suggested to contribute to defective disk membrane morphogenesis that is manifest by overgrown nascent disks (Williams et al., 1988). Loss of PCDH15 or CDH23, the USH1F and USH1D proteins, also results in loss of f-actin in the calycal processes and the same perturbed disk morphogenesis phenotype (Schietroma et al., 2017). Hence, the calycal process localization of USH1 proteins may be important in USH1 retinal pathology (Sahly et al., 2012, Schietroma et al., 2017), although, to date, no mutant phenotype has been linked to the calycal processes due to lack of MYO7A.

We found the expression of *Myo7a* IF1 to be more similar to that of IF2, in mouse NR, than in pig or human NR, where IF2 is clearly the more abundant isoform (Fig. 2). These results were confirmed using a second set of mouse IF1 primers. It is tempting to suggest that this difference in isoform expression might be related to a difference between mouse and human in the subcellular structures that contain MYO7A, combined with different subcellular distributions for IF1 and IF2. However, photoreceptors in retinal organoids do not appear to have well-developed calycal processes, even in the few cases where disk membranes (rather than membrane tubules) have clearly formed (Zhong et al., 2014, West et al., 2022). Yet, the IF1 to IF2 ratio was similar between human retinal organoids and the

other human retinal tissues (Fig. 2), suggesting no relationship between isoform expression and photoreceptor subcellular structures.

Supplementary Material

Refer to Web version on PubMed Central for supplementary material.

Acknowledgements

We thank Agrani Rump for initial work on this project, Barry Burgess for technical support, and Roni Hazim, Antonio Paniagua, and Simona Torriano for helpful comments on the project and manuscript. We are also grateful to Ariel Ben-Sasson for helpful discussions about the 3D modeling of MYO7A. The study was supported by NIH NEI grants R01EY027442, R01EY033035, R21EY031109 and P30EY00333, and a program project grant from the Foundation Fighting Blindness (DSW); by NIH NEI postdoctoral fellowship F32EY031575 (NWH); and by the Gates Frontiers Fund, The Solich Fund, *CellSight* Development Fund, and an unrestricted grant to the Department of Ophthalmology, University of Colorado from Research to Prevent Blindness (MVC-S).

References

Adato A, Michel V, Kikkawa Y, Reiners J, Alagramam KN, Weil D, Yonekawa H, Wolfrum U, El-Amraoui A, & Petit C (2005). Interactions in the network of Usher syndrome type 1 proteins. Hum Mol Genet, 14 (3), 347–356. [PubMed: 15590703]

Aparicio-Domingo S, Flores-Bellver M, Cobb H, Li KV, Conrad B, Chen C, Brzezinski JA, & Canto-Soler MV (2023). Generation of Three-Dimensional Retinal Tissue with Physiologically Competent, Light-Sensitive Photoreceptors from Human-Induced Pluripotent Stem Cells. In: Gopalakrishnan J (Ed.) Brain Organoid Research (pp. 99–119). New York, NY: Springer US.

Arikawa K, Molday LL, Molday RS, & Williams DS (1992). Localization of peripherin/rds in the disk membranes of cone and rod photoreceptors: relationship to disk membrane morphogenesis and retinal degeneration. J Cell Biol, 116 (3), 659–667. [PubMed: 1730772]

Berger W, Kloeckener-Gruissem B, & Neidhardt J (2010). The molecular basis of human retinal and vitreoretinal diseases. Prog Retin Eye Res, 29 (5), 335–375. [PubMed: 20362068]

Brown PK, Gibbons IR, & Wald G (1963). The Visual Cells and Visual Pigment of the Mudpuppy, Necturus. J Cell Biol, 19 (1), 79–106. [PubMed: 14069804]

Buchholz DE, Pennington BO, Croze RH, Hinman CR, Coffey PJ, & Clegg DO (2013). Rapid and efficient directed differentiation of human pluripotent stem cells into retinal pigmented epithelium. Stem Cells Transl Med, 2 (5), 384–393. [PubMed: 23599499]

Burridge PW, Thompson S, Millrod MA, Weinberg S, Yuan X, Peters A, Mahairaki V, Koliatsos VE, Tung L, & Zambidis ET (2011). A universal system for highly efficient cardiac differentiation of human induced pluripotent stem cells that eliminates interline variability. PLoS One, 6 (4), e18293. [PubMed: 21494607]

Calabro KR, Boye SL, Choudhury S, Fajardo D, Peterson JJ, Li W, Crosson SM, Kim MJ, Ding D, Salvi R, Someya S, & Boye SE (2019). A Novel Mouse Model of MYO7A USH1B Reveals Auditory and Visual System Haploinsufficiencies. Front Neurosci, 13, 1255. [PubMed: 31824252]

Castiglione A, & Moller C (2022). Usher Syndrome. Audiol Res, 12 (1), 42–65. [PubMed: 35076463]

Cehajic-Kapetanovic J, Xue K, Martinez-Fernandez de la Camara C, Nanda A, Davies A, Wood LJ, Salvetti AP, Fischer MD, Aylward JW, Barnard AR, Jolly JK, Luo E, Lujan BJ, Ong T, Girach A, Black GCM, Gregori NZ, Davis JL, Rosa PR, Lotery AJ, Lam BL, Stanga PE, & MacLaren RE (2020). Initial results from a first-in-human gene therapy trial on X-linked retinitis pigmentosa caused by mutations in RPGR. Nat Med, 26 (3), 354–359. [PubMed: 32094925]

Chishti AH, Kim AC, Marfatia SM, Lutchman M, Hanspal M, Jindal H, Liu SC, Low PS, Rouleau GA, Mohandas N, Chasis JA, Conboy JG, Gascard P, Takakuwa Y, Huang SC, Benz EJ Jr., Bretscher A, Fehon RG, Gusella JF, Ramesh V, Solomon F, Marchesi VT, Tsukita S, Tsukita S, Hoover KB, & et al. (1998). The FERM domain: a unique module involved in the linkage of cytoplasmic proteins to the membrane. Trends Biochem Sci, 23 (8), 281–282. [PubMed: 9757824]

Cideciyan AV, Jacobson SG, Beltran WA, Sumaroka A, Swider M, Iwabe S, Roman AJ, Olivares MB, Schwartz SB, Komaromy AM, Hauswirth WW, & Aguirre GD (2013). Human retinal gene therapy for Leber congenital amaurosis shows advancing retinal degeneration despite enduring visual improvement. Proc Natl Acad Sci U S A, 110 (6), E517–525. [PubMed: 23341635]

Colella P, Sommella A, Marrocco E, Di Vicino U, Polishchuk E, Garrido MG, Seeliger MW, Polishchuk R, & Auricchio A (2013). Myosin7a deficiency results in reduced retinal activity which is improved by gene therapy. PloS one, 8 (8), e72027. [PubMed: 23991031]

Colella P, Trapani I, Cesi G, Sommella A, Manfredi A, Puppo A, Iodice C, Rossi S, Simonelli F, Giunti M, Bacci ML, & Auricchio A (2014). Efficient gene delivery to the cone-enriched pig retina by dual AAV vectors. Gene Ther, 21 (4), 450–456. [PubMed: 24572793]

El-Amraoui A, Sahly I, Picaud S, Sahel J, Abitbol M, & Petit C (1996). Human Usher 1B/mouse shaker-1: the retinal phenotype discrepancy explained by the presence/absence of myosin VIIA in the photoreceptor cells. Hum Mol Genet, 5 (8), 1171–1178. [PubMed: 8842737]

El-Amraoui A, Schonn JS, Kussel-Andermann P, Blanchard S, Desnos C, Henry JP, Wolfrum U, Darchen F, & Petit C (2002). MyRIP, a novel Rab effector, enables myosin VIIa recruitment to retinal melanosomes. EMBO Rep, 3 (5), 463–470. [PubMed: 11964381]

Esteve-Rudd J, Hazim RA, Diemer T, Paniagua AE, Volland S, Umapathy A, & Williams DS (2018). Defective phagosome motility and degradation in cell nonautonomous RPE pathogenesis of a dominant macular degeneration. Proc Natl Acad Sci U S A, 115 (21), 5468–5473. [PubMed: 29735674]

Ferla R, Dell'Aquila F, Doria M, Ferraiuolo M, Noto A, Grazioli F, Ammendola V, Testa F, Melillo P, Iodice C, Risca G, Tedesco N, le Brun PR, Surace EM, Simonelli F, Galimberti S, Valsecchi MG, Marteau JB, Veron P, Colloca S, & Auricchio A (2023). Efficacy, pharmacokinetics, and safety in the mouse and primate retina of dual AAV vectors for Usher syndrome type 1B. Mol Ther Methods Clin Dev, 28, 396–411. [PubMed: 36910588]

Fischer MD, Michalakis S, Wilhelm B, Zobor D, Muehlfriedel R, Kohl S, Weisschuh N, Ochakovski GA, Klein R, Schoen C, Sothilingam V, Garcia-Garrido M, Kuehlewein L, Kahle N, Werner A, Dauletbekov D, Paquet-Durand F, Tsang S, Martus P, Peters T, Seeliger M, Bartz-Schmidt KU, Ueffing M, Zrenner E, Biel M, & Wissinger B (2020). Safety and Vision Outcomes of Subretinal Gene Therapy Targeting Cone Photoreceptors in Achromatopsia: A Nonrandomized Controlled Trial. JAMA Ophthalmol, 138 (6), 643–651. [PubMed: 32352493]

Flores-Bellver M, Mighty J, Aparicio-Domingo S, Li KV, Shi C, Zhou J, Cobb H, McGrath P, Michelis G, Lenhart P, Bilousova G, Heissel S, Rudy MJ, Coughlan C, Goodspeed AE, Becerra SP, Redenti S, & Canto-Soler MV (2021). Extracellular vesicles released by human retinal pigment epithelium mediate increased polarised secretion of drusen proteins in response to AMD stressors. J Extracell Vesicles, 10 (13), e12165. [PubMed: 34750957]

Fukuda M, & Kuroda TS (2002). Slac2-c (synaptotagmin-like protein homologue lacking C2 domains-c), a novel linker protein that interacts with Rab27, myosin Va/VIIa, and actin. J Biol Chem, 277 (45), 43096–43103. [PubMed: 12221080]

Futter CE, Ramalho JS, Jaissle GB, Seeliger MW, & Seabra MC (2004). The role of Rab27a in the regulation of melanosome distribution within retinal pigment epithelial cells. Mol Biol Cell, 15 (5), 2264–2275. [PubMed: 14978221]

Gibbs D, Azarian SM, Lillo C, Kitamoto J, Klomp AE, Steel KP, Libby RT, & Williams DS (2004). Role of myosin VIIa and Rab27a in the motility and localization of RPE melanosomes. J Cell Sci, 117 (Pt 26), 6473–6483. [PubMed: 15572405]

Gibbs D, Diemer T, Khanobdee K, Hu J, Bok D, & Williams DS (2010). Function of MYO7A in the human RPE and the validity of shaker1 mice as a model for Usher syndrome 1B. Invest Ophthalmol Vis Sci, 51 (2), 1130–1135. [PubMed: 19643958]

Gibbs D, Kitamoto J, & Williams DS (2003). Abnormal phagocytosis by retinal pigmented epithelium that lacks myosin VIIa, the Usher syndrome 1B protein. Proc Natl Acad Sci U S A, 100 (11), 6481–6486. [PubMed: 12743369]

Gordiyenko NV, Fariss RN, Zhi C, & MacDonald IM (2010). Silencing of the CHM gene alters phagocytic and secretory pathways in the retinal pigment epithelium. Investigative ophthalmology & visual science, 51 (2), 1143–1150. [PubMed: 19741243]

Gu SM, Thompson DA, Srikumari CR, Lorenz B, Finckh U, Nicoletti A, Murthy KR, Rathmann M, Kumaramanickavel G, Denton MJ, & Gal A (1997). Mutations in RPE65 cause autosomal recessive childhood-onset severe retinal dystrophy. Nat Genet, 17 (2), 194–197. [PubMed: 9326941]

Hashimoto T, Gibbs D, Lillo C, Azarian SM, Legacki E, Zhang XM, Yang XJ, & Williams DS (2007). Lentiviral gene replacement therapy of retinas in a mouse model for Usher syndrome type 1B. Gene therapy, 14 (7), 584–594. [PubMed: 17268537]

Hasson T (2000). Personal Communication.

Hasson T, Heintzelman MB, Santos-Sacchi J, Corey DP, & Mooseker MS (1995). Expression in cochlea and retina of myosin VIIa, the gene product defective in Usher syndrome type 1B. Proc. Natl. Acad. Sci. USA, 92, 9815–9819. [PubMed: 7568224]

Hazim RA, Karumbayaram S, Jiang M, Dimashkie A, Lopes VS, Li D, Burgess BL, Vijayaraj P, Alva-Ornelas JA, Zack JA, Kohn DB, Gomperts BN, Pyle AD, Lowry WE, & Williams DS (2017). Differentiation of RPE cells from integration-free iPS cells and their cell biological characterization. Stem Cell Res Ther, 8 (1), 217. [PubMed: 28969679]

Hazim RA, Paniagua AE, Tang L, Yang K, Kim KKO, Stiles L, Divakaruni AS, & Williams DS (2022). Vitamin B3, nicotinamide, enhances mitochondrial metabolism to promote differentiation of the retinal pigment epithelium. J Biol Chem, 298 (9), 102286. [PubMed: 35868562]

Hazim RA, Volland S, Yen A, Burgess BL, & Williams DS (2019). Rapid differentiation of the human RPE cell line, ARPE-19, induced by nicotinamide. Exp Eye Res, 179, 18–24. [PubMed: 30336127]

Hogan MJ, Alvarado JA, & Weddell JE (1971). Histology of the human eye: An atlas and textbook. (Saunders.

Jacobson SG, Cideciyan AV, Aleman TS, Sumaroka A, Roman AJ, Gardner LM, Prosser HM, Mishra M, Bech-Hansen NT, Herrera W, Schwartz SB, Liu XZ, Kimberling WJ, Steel KP, & Williams DS (2008). Usher syndromes due to MYO7A, PCDH15, USH2A or GPR98 mutations share retinal disease mechanism. Human molecular genetics, 17 (15), 2405–2415. [PubMed: 18463160]

Jacobson SG, Cideciyan AV, Gibbs D, Sumaroka A, Roman AJ, Aleman TS, Schwartz SB, Olivares MB, Russell RC, Steinberg JD, Kenna MA, Kimberling WJ, Rehm HL, & Williams DS (2011). Retinal disease course in Usher syndrome 1B due to MYO7A mutations. Invest Ophthalmol Vis Sci, 52 (11), 7924–7936. [PubMed: 21873662]

Jiang M, Esteve-Rudd J, Lopes VS, Diemer T, Lillo C, Rump A, & Williams DS (2015). Microtubule motors transport phagosomes in the RPE, and lack of KLC1 leads to AMD-like pathogenesis. J Cell Biol, 210 (4), 595–611. [PubMed: 26261180]

Kessel RG, & Kardon RH (1979). Nervous tissue - eye and ear. In: Kessel RG (Ed.) A text atlas of scanning electron microscopy (San Francisco: W.H. Freeman.

Klomp AE, Teofilo K, Legacki E, & Williams DS (2007). Analysis of the linkage of MYRIP and MYO7A to melanosomes by RAB27A in retinal pigment epithelial cells. Cell Motil Cytoskeleton, 64 (6), 474–487. [PubMed: 17352418]

Krock BL, Bilotta J, & Perkins BD (2007). Noncell-autonomous photoreceptor degeneration in a zebrafish model of choroideremia. Proc Natl Acad Sci U S A, 104 (11), 4600–4605. [PubMed: 17360570]

Leong YC, Di Foggia V, Pramod H, Bitner-Glindzicz M, Patel A, & Sowden JC (2022). Molecular pathology of Usher 1B patient-derived retinal organoids at single cell resolution. Stem Cell Reports, 17 (11), 2421–2437. [PubMed: 36240775]

Libby RT, & Steel KP (2001). Electroretinographic anomalies in mice with mutations in Myo7a, the gene involved in human Usher syndrome type 1B. Invest Ophthalmol Vis Sci, 42 (3), 770–778. [PubMed: 11222540]

Liu X, Ondek B, & Williams DS (1998). Mutant myosin VIIa causes defective melanosome distribution in the RPE of shaker-1 mice. Nat. Genet, 19 (2), 117–118. [PubMed: 9620764]

Liu X, Udovichenko IP, Brown SD, Steel KP, & Williams DS (1999). Myosin VIIa participates in opsin transport through the photoreceptor cilium. J Neurosci, 19 (15), 6267–6274. [PubMed: 10414956]

Liu X, Vansant G, Udovichenko IP, Wolfrum U, & Williams DS (1997). Myosin VIIa, the product of the Usher 1B syndrome gene, is concentrated in the connecting cilia of photoreceptor cells. Cell Motil Cytoskeleton, 37 (3), 240–252. [PubMed: 9227854]

Lopes VS, Boye SE, Louie CM, Boye S, Dyka F, Chiodo V, Fofo H, Hauswirth WW, & Williams DS (2013). Retinal gene therapy with a large MYO7A cDNA using adeno-associated virus. Gene therapy, 20 (8), 824–833. [PubMed: 23344065]

Lopes VS, Gibbs D, Libby RT, Aleman TS, Welch DL, Lillo C, Jacobson SG, Radu RA, Steel KP, & Williams DS (2011). The Usher 1B protein, MYO7A, is required for normal localization and function of the visual retinoid cycle enzyme, RPE65. Hum Mol Genet

Lopes VS, Ramalho JS, Owen DM, Karl MO, Strauss O, Futter CE, & Seabra MC (2007). The ternary Rab27a-Myrip-Myosin VIIa complex regulates melanosome motility in the retinal pigment epithelium. Traffic, 8 (5), 486–499. [PubMed: 17451552]

Mullen RJ, & LaVail MM (1976). Inherited retinal dystrophy: primary defect in pigment epithelium determined with experimental rat chimeras. Science, 192 (4241), 799–801. [PubMed: 1265483]

Rakoczy EP, Magno AL, Lai CM, Pierce CM, Degli-Esposti MA, Blumenkranz MS, & Constable IJ (2019). Three-Year Follow-Up of Phase 1 and 2a rAAV.sFLT-1 Subretinal Gene Therapy Trials for Exudative Age-Related Macular Degeneration. Am J Ophthalmol, 204, 113–123. [PubMed: 30878487]

Rakoczy PE, Zhang D, Robertson T, Barnett NL, Papadimitriou J, Constable IJ, & Lai CM (2002). Progressive age-related changes similar to age-related macular degeneration in a transgenic mouse model. Am J Pathol, 161 (4), 1515–1524. [PubMed: 12368224]

Reichenbach A, Stolzenburg JU, Eberhardt W, Chao TI, Dettmer D, & Hertz L (1993). What do retinal muller (glial) cells do for their neuronal 'small siblings'? J Chem Neuroanat, 6 (4), 201–213. [PubMed: 8104418]

Reiners J, van Wijk E, Marker T, Zimmermann U, Jurgens K, te Brinke H, Overlack N, Roepman R, Knipper M, Kremer H, & Wolfrum U (2005). Scaffold protein harmonin (USH1C) provides molecular links between Usher syndrome type 1 and type 2. Hum Mol Genet, 14 (24), 3933–3943. [PubMed: 16301216]

Russell S, Bennett J, Wellman JA, Chung DC, Yu ZF, Tillman A, Wittes J, Pappas J, Elci O, McCague S, Cross D, Marshall KA, Walshire J, Kehoe TL, Reichert H, Davis M, Raffini L, George LA, Hudson FP, Dingfield L, Zhu X, Haller JA, Sohn EH, Mahajan VB, Pfeifer W, Weckmann M, Johnson C, Gewaily D, Drack A, Stone E, Wachtel K, Simonelli F, Leroy BP, Wright JF, High KA, & Maguire AM (2017). Efficacy and safety of voretigene neparvovec (AAV2-hRPE65v2) in patients with RPE65-mediated inherited retinal dystrophy: a randomised, controlled, open-label, phase 3 trial. Lancet, 390 (10097), 849–860. [PubMed: 28712537]

Sahly I, Dufour E, Schietroma C, Michel V, Bahloul A, Perfettini I, Pepermans E, Estivalet A, Carette D, Aghaie A, Ebermann I, Lelli A, Iribarne M, Hardelin JP, Weil D, Sahel JA, El-Amraoui A, & Petit C (2012). Localization of Usher 1 proteins to the photoreceptor calyceal processes, which are absent from mice. J Cell Biol, 199 (2), 381–399. [PubMed: 23045546]

Schietroma C, Parain K, Estivalet A, Aghaie A, Boutet de Monvel J, Picaud S, Sahel JA, Perron M, El-Amraoui A, & Petit C (2017). Usher syndrome type 1-associated cadherins shape the photoreceptor outer segment. J Cell Biol, 216 (6), 1849–1864. [PubMed: 28495838]

Schwander M, Lopes V, Sczaniecka A, Gibbs D, Lillo C, Delano D, Tarantino LM, Wiltshire T, Williams DS, & Muller U (2009). A novel allele of myosin VIIa reveals a critical function for the C-terminal FERM domain for melanosome transport in retinal pigment epithelial cells. J Neurosci, 29 (50), 15810–15818. [PubMed: 20016096]

Sorusch N, Yildirim A, Knapp B, Janson J, Fleck W, Scharf C, & Wolfrum U (2019). SANS (USH1G) Molecularly Links the Human Usher Syndrome Protein Network to the Intraflagellar Transport Module by Direct Binding to IFT-B Proteins. Front Cell Dev Biol, 7, 216. [PubMed: 31637240]

Steinberg RH, Fisher SK, & Anderson DH (1980). Disc morphogenesis in vertebrate photoreceptors. J. Comp. Neurol, 190 (3), 501–508. [PubMed: 6771304]

Trapani I, Colella P, Sommella A, Iodice C, Cesi G, de Simone S, Marrocco E, Rossi S, Giunti M, Palfi A, Farrar GJ, Polishchuk R, & Auricchio A (2014). Effective delivery of large genes to the retina by dual AAV vectors. EMBO molecular medicine, 6 (2), 194–211. [PubMed: 24150896]

Udovichenko IP, Gibbs D, & Williams DS (2002). Actin-based motor properties of native myosin VIIa. J Cell Sci, 115 (Pt 2), 445–450. [PubMed: 11839794]

Volland S, Hughes LC, Kong C, Burgess BL, Linberg KA, Luna G, Zhou ZH, Fisher SK, & Williams DS (2015). Three-dimensional organization of nascent rod outer segment disk membranes. Proc Natl Acad Sci U S A

Weil D, Blanchard S, Kaplan J, Guilford P, Gibson F, Walsh J, Mburu P, Varela A, Levilliers J, Weston MD, Kelley PM, Kimberling WJ, Wagenaar M, Levi-Acobas F, Larget-Piet D, Munnich A, Steel KP, Brown SDM, & Petit C (1995). Defective myosin VIIA gene responsible for Usher syndrome type 1B. Nature, 374, 60–61. [PubMed: 7870171]

Weil D, El-Amraoui A, Masmoudi S, Mustapha M, Kikkawa Y, Laine S, Delmaghani S, Adato A, Nadifi S, Zina BZ, Hamel C, Gal A, Ayadi H, Yonekawa H, & Petit C (2003). Usher syndrome type I G (USH1G) is caused by mutations in the gene encoding SANS, a protein that associates with the USH1C protein, harmonin. Human Mol Genet, 12 (5), 463–471. [PubMed: 12588794]

Weil D, Levy G, Sahly I, Levi-Acobas F, Blanchard S, El-Amraoui A, Crozet F, Philippe H, Abitbol M, & Petit C (1996). Human myosin VIIA responsible for the Usher 1B syndrome: a predicted membrane-associated motor protein expressed in developing sensory epithelia. Proc Natl Acad Sci U S A, 93 (8), 3232–3237. [PubMed: 8622919]

West EL, Majumder P, Naeem A, Fernando M, O'Hara-Wright M, Lanning E, Kloc M, Ribeiro J, Ovando-Roche P, Shum IO, Jumbu N, Sampson R, Hayes M, Bainbridge JWB, Georgiadis A, Smith AJ, Gonzalez-Cordero A, & Ali RR (2022). Antioxidant and lipid supplementation improve the development of photoreceptor outer segments in pluripotent stem cell-derived retinal organoids. Stem Cell Reports, 17 (4), 775–788. [PubMed: 35334217]

Williams DS (2008). Usher syndrome: Animal models, retinal function of Usher proteins, and prospects for gene therapy. Vision Res, 48 (3), 433–441. [PubMed: 17936325]

Williams DS, Chadha A, Hazim R, & Gibbs D (2017). Gene therapy approaches for prevention of retinal degeneration in Usher syndrome. Gene Ther, 24 (2), 68–71. [PubMed: 28054582]

Williams DS, Linberg KA, Vaughan DK, Fariss RN, & Fisher SK (1988). Disruption of microfilament organization and deregulation of disk membrane morphogenesis by cytochalasin D in rod and cone photoreceptors. J Comp Neurol, 272 (2), 161–176. [PubMed: 3397406]

Williams DS, & Lopes VS (2011). The many different cellular functions of MYO7A in the retina. Biochemical Society transactions, 39 (5), 1207–1210. [PubMed: 21936790]

Wolfrum U, & Schmitt A (2000). Rhodopsin transport in the membrane of the connecting cilium of mammalian photoreceptor cells. Cell Motil Cytoskeleton, 46 (2), 95–107. [PubMed: 10891855]

Yan AL, Du SW, & Palczewski K (2023). Genome editing, a superior therapy for inherited retinal diseases. Vision Res, 206, 108192. [PubMed: 36804635]

Yu-Wai-Man P, Newman NJ, Carelli V, Moster ML, Biousse V, Sadun AA, Klopstock T, Vignal-Clermont C, Sergott RC, Rudolph G, La Morgia C, Karanjia R, Taiel M, Blouin L, Burguiere P, Smits G, Chevalier C, Masonson H, Salermo Y, Katz B, Picaud S, Calkins DJ, & Sahel JA (2020). Bilateral visual improvement with unilateral gene therapy injection for Leber hereditary optic neuropathy. Sci Transl Med, 12 (573)

Zhong X, Gutierrez C, Xue T, Hampton C, Vergara MN, Cao LH, Peters A, Park TS, Zambidis ET, Meyer JS, Gamm DM, Yau KW, & Canto-Soler MV (2014). Generation of three-dimensional retinal tissue with functional photoreceptors from human iPSCs. Nat Commun, 5, 4047. [PubMed: 24915161]

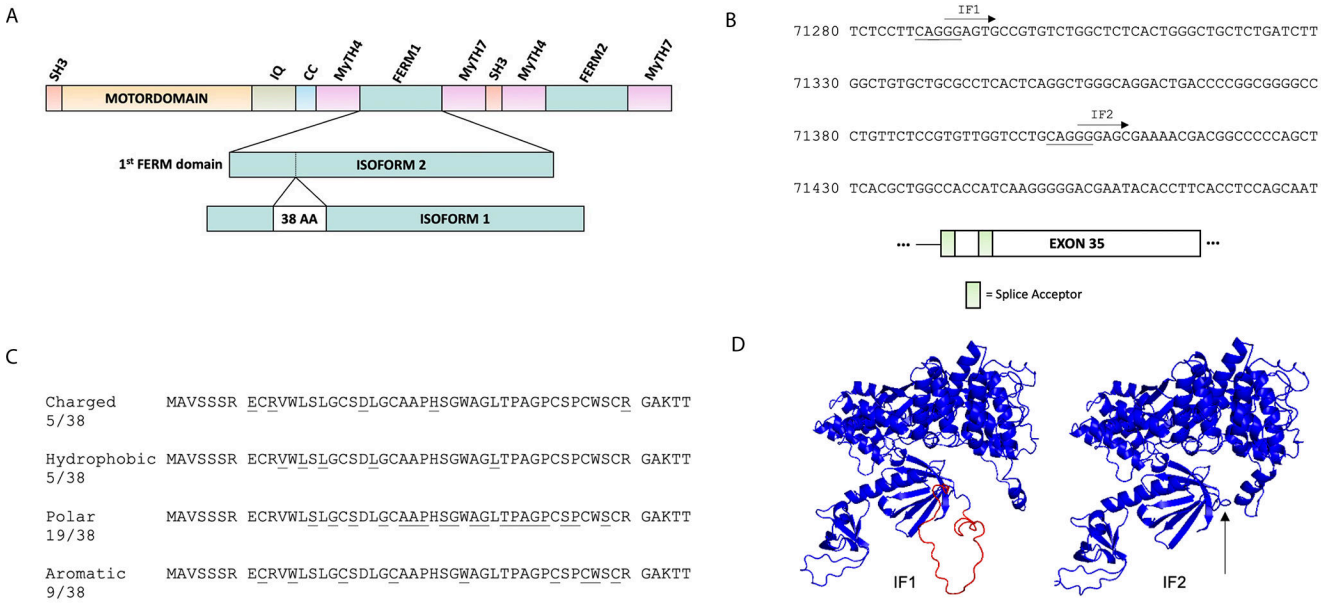

Fig. 1.

The two retinal isoforms of MYO7A. (A) Schematic of MYO7A, illustrating the major domains of the polypeptide and the difference between the two retinal isoforms, which consists of the presence or absence of a 38 amino acid sequence within the FERM1 domain. (B) Depiction of the two putative IF1/IF2 splice acceptors that are associated with exon 35. The end of each putative splice acceptor sequence (YnNCAGGG) is underlined, and the first 6 nucleotides of each isoform coding region is marked with a directional arrow. (C) Amino acids of the 38 amino acid sequence that is unique to IF1, identified by class. (D) 3D modeling of the FERM1 domain of human MYO7A IF1 and IF2. The additional 38 amino acids at the C lobe of the FERM1 domain of IF1 are marked in red, and the location where they are missing in IF2 is marked with an arrow.

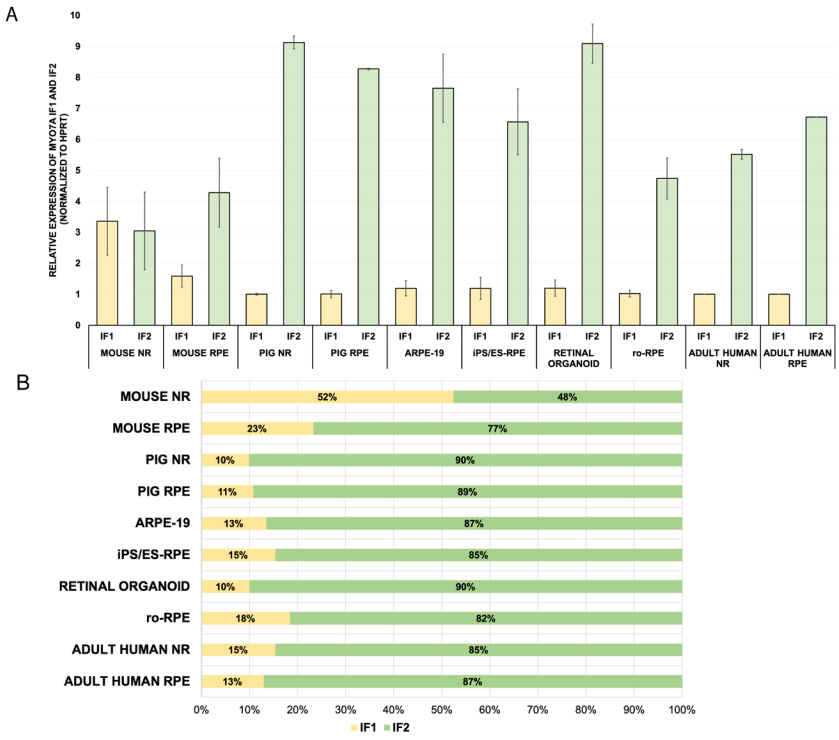

Fig. 2.

Quantitative PCR measurements of the expression of the two retinal *Myo7a*/*MYO7A* isoforms in different neural retina (NR) and RPE samples. (A) Graph comparing IF1 and IF2 expression for each tissue sample. Because HPRT expression likely varies among the different tissues, quantitative comparisons should not be made among the tissue samples. Mean values of biological replicates (Table 1) are plotted with error bars representing ± SEM. (B) Measurements of the expression of each isoform shown as a percentage of the expression for each tissue sample.

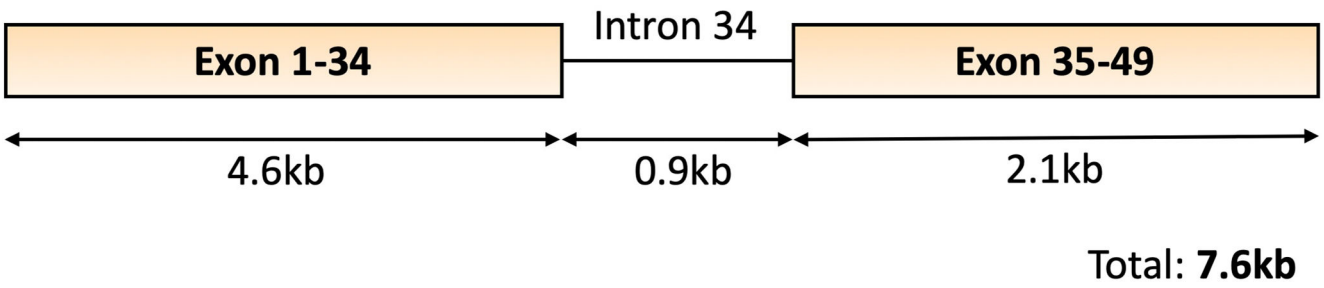

Fig. 3.

Suggested construct design that would potentially generate both IF1 and IF2 MYO7A isoforms in gene augmentation therapy.

Table 1.

Quantitative PCR samples

	Mouse NR	Mouse RPE	Pig NR	Pig RPE	ARPE-19	iPS/ES-RPE	Retinal Organoid	ro-RPE	Adult Human NR	Adult Human RPE
gender	M+F	M+F	F	F	M	M+F	F	F	M+F	M
no. of subjects *	11	4	1	1	-	-	-	-	2	1
no. of separate samples (n value)	11	4	2	2	7	6	5	4	2	1
#no. of qPCR reactions per sample	3–4	6–9	6	6	4–6	3–8	3–6	3–6	3	3

* Two eyes were collected from each mouse or pig. Each pair of mouse eyes was pooled.